Exploring RF Transmissions From Discharge-Based Micromachined Radiation Detectors

Christine K. Eun[1] and Yogesh B. Gianchandani
NSF Engineering Research Center for Wireless Integrated Microsystems (WIMS)
Department of Electrical Engineering and Computer Science, University of Michigan
[1]1301 Beal Avenue, Ann Arbor, Michigan, USA, e-mail: eunc@umich.edu

Abstract—*This paper describes micromachined gas-based radiation sensors that are capable of radio frequency wireless signaling, and their possible utility in networks. The devices include a gas-filled region with a high electric field, in which incident beta-particles initiate avalanche breakdown. Under the proper circumstances, the resulting current pulses can inherently produce wireless transmissions. Two types of lithographically-manufactured devices are presented: (1) a silicon/glass stack with etched detection cavities and (2) a planar, 3-electrode metal-on-glass structure that uses a high-impedance electrode for increased control of discharge energy. Both are capable of producing ultra-wideband signals spanning >2.9 GHz. Permanent magnets (integrated with both structures) can enhance the RF performance by ≈15-20 dBμV. The impact of operating pressure, fill-gases (which are typically a mixture of Ne and N_2) and electrode materials (Ni, Cu) on device performance is described. Tests performed in the proximity of weak (0.1–1.0 μCi) beta sources (^{90}Sr, ^{204}Tl), show that a 25% decrease in pressure permits a 55% decrease in operating voltage. Increasing Ne content in the fill-gas (e.g. Ne-to-N_2 ratio from 1:5 to 3:5) decreases the minimum operating voltage by 200 V without loss in RF performance. Ni electrodes, which have a higher secondary electron emission coefficient than Cu, provide 30% more overall signal power.*

1. Introduction

Miniaturized radiation sensors with wireless signaling capability can be useful both in networks and as individual devices. As elements of a network, they can facilitate cost-effective sensing in public spaces (e.g. football stadiums, amusement parks, and shopping malls), or in dangerous and inaccessible environments (e.g. contaminated or remote areas). Individually, they could be used in applications for which the weight or space is at a premium, e.g. micro-air-vehicles (MAVs), or helmets. In general, such devices offer high portability, minimal power demands, and modest manufacturing costs.

Wireless-capability in micro-sensor networks can facilitate rapid deployment and reconfiguration. They can be integrated discreetly in the side of buildings or passageways. Past work on wireless-enabled detector networks have included the use of multiple 75 mm NaI scintillators connected to PDA-sized platforms that are linked to mote gateways [1] and arrays of 2”X2” radiation detectors communicating via wireless mesh routing protocols [2]. Both require radiation-shielded transponders at each sensor node.

In one possible configuration (Fig. 1), the wireless micro-sensors are distributed in clusters – locations A, B…. Within each cluster, there are a number of functionally identical individual sensors that are interchangeable, transmitting on the same frequency bands. Each cluster communicates to a localized-transponder (LT), which reports to a centralized master-control-module (MCM). A possible application is the monitoring of a large cargo ship (Fig. 2), with each shipping container housing a sensor cluster and LT, and the MCM located at the helm.

Gas-based detectors (e.g. Geiger counters) tend to be favored for environmental surveillance efforts (i.e. in

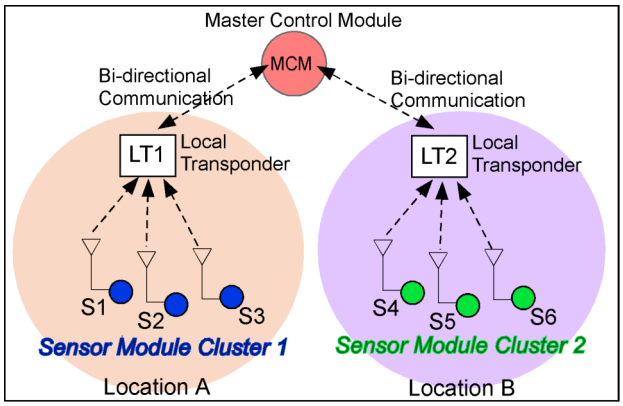

Fig. 1: A possible network configuration plan includes multiple clusters of sensor modules transmitting to a localized transponder (LT) that has bi-directional communication capability with the master control module (MCM). Each sensor module (S1, S2, S3...) can transmit on identical frequency bands, which allows instantaneous changes in cluster size and configuration without changes to the LT or MCM.

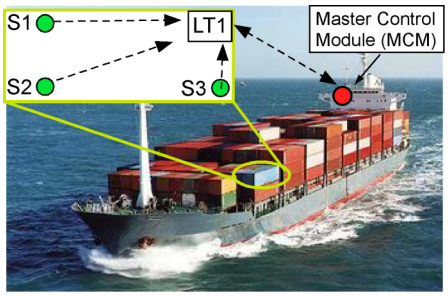

Fig. 2: Network configuration plan applied to a cargo container ship scenario.

looking for radiation leaks and inadvertent contamination) [3], because they tend to be stable, temperature insensitive, require only simple circuitry, and can sense a wide range of radiation species and energies. The miniaturization of gas-based detectors can permit the use of lithographic manufacturing to drive down sensor cost. In addition, smaller sensor dimensions allow for the formation of composite sensor structures, which can increase overall functionality. Finally, scaling down feature sizes and electrode spacing can lead to increased resolution in imaging applications [4]. Typically, gas-based detectors involve biased electrodes (anode and cathode) surrounded by an enclosed gas mixture. Ionizing radiation interacts with the gas, forming ions and electrons, which are then accelerated by the applied field. They initiate electron avalanches that lead to current discharges, which amplify the signal that is collected at the anode. These discharges can concomitantly produce a wireless signal, demonstrating the potential for wireless detection of radioactive chemicals.

Gas-based discharges were employed for wireless communication in the mid-1890's using Marconi's spark gap transmitters [5]. The discharge gaps were relatively large (on the order of cm), achieving transmission distances on the order of kilometers. In 1901, Bose utilized these discharges within waveguides in order to generate microwaves. More recent activity on this topic has been reported [6].

This paper presents two types of lithographically-manufactured radiation sensors (Design A, Design B) that employ micro-discharges to generate radio-frequency signals in the ultra wideband (UWB) frequency range. Section 2 introduces the 2-electrode Si/glass micro-detector (Design A), followed by fabrication details and experimental results. Section 3 describes the power saving operation achieved with the planar, 3-electrode design (Design B). Section 4 describes how wireless signal enhancement is possible by incorporating permanent magnets in both structures. Finally, Section 5 describes the effects of electrode materials and fill-gases on the RF characteristics.

2. MICRO-DETECTOR - DESIGN A

Device Concept

Design A is a 2-electrode, Si-glass, stacked configuration, as shown in Fig. 3, and is intended primarily for beta-particle detection. Each sensor cavity has a square chamber with a central cathode and a peripheral anode. The region proximal to the cathode has a weak field and is called the drift region, whereas that adjacent to the anode is the high-field amplification region. As beta-particles enter the cavity, they ionize the surrounding gas. (In contrast with conventional Geiger counters, this gas is at atmospheric pressure.) The electrons are swept from the drift region into the amplification region, where they are quickly accelerated into avalanche breakdown. This results in a micro-discharge and RF transmission. Designing the drift region to be much larger than the amplification region permits pulses to be relatively independent of the entry position of the radiation.

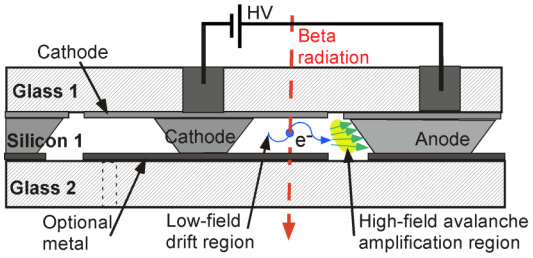

(a)

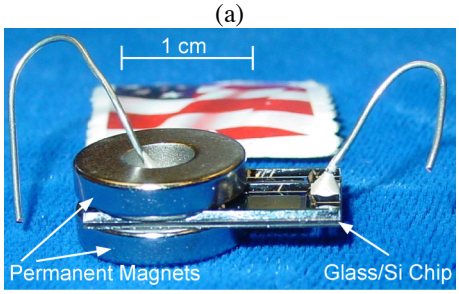

(b)

Fig. 3: (a) Cross-section of **Design A**. (b) Photograph of Design A with additional permanent magnets (explained in Sec. 4). This microchip contains 6 individual gas-filled cavities with areas ranging in size from 3 mm^2 to 64 mm^2.

Fabrication

Design A is fabricated in a simple, two-mask (or optional three-mask) process (Fig. 4). Beginning with a 500 μm-thick <100> Si wafer, Mask 1 defines the boron diffusion profile for the central cathode and anode. Boron is diffused 8 μm-deep and is used as an etch stop later in the process. The Si wafer is anodically bonded to a 500 μm-thick Pyrex glass wafer. Next, SiO_2 is grown and patterned using Mask 2. This will define the Si anode wall structure. The <111> walls of the silicon are anisotropically wet-etched using ethylene diamine and pyrocatechol (EDP), which forms the cavity structures, defines the anode wall, and exposes the boron-doped cathodes. A glass window stacked on top of the cavities completes the device. An optional masking step defines a metal pattern on the glass window intended for eutectic bonding methods for wafer-level gas packaging.

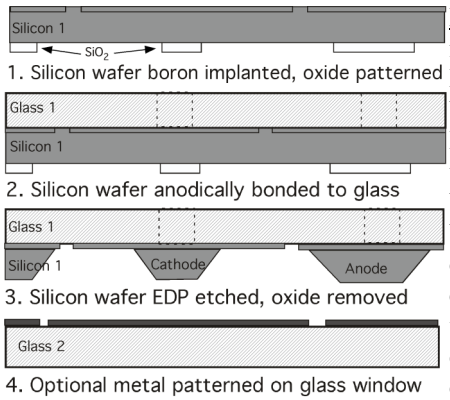

Fig. 4: Process flow for Design A. Mask 1 defines a boron etch stop, Mask 2 patterns the oxide. Anodic bonding followed by EDP etching define the device cavity. A glass window is stacked on top of the detector structure.

Experimental Results

A configuration of the kind shown in Fig. 5 is used to characterize these devices. A gas-controlled test chamber permits the trial of a variety of fill-gases encapsulated within the sensor cavity, which remains unsealed for the purpose of testing. Low-level sealed sources – ^{90}Sr and ^{204}Tl with 0.1-1.0 μCi strengths – are located within the chamber. An 8X8 mm^2 detection cavity has measured count rates on the order of 10^3 counts-per-minute (Fig. 6). The sensitivity (cpm/mRad/hr) of Design A is about 70% that of commercial radiation detectors when normalized to the detector area. However, the micro-detector occupies only about 0.06% of the conventional detector volume.

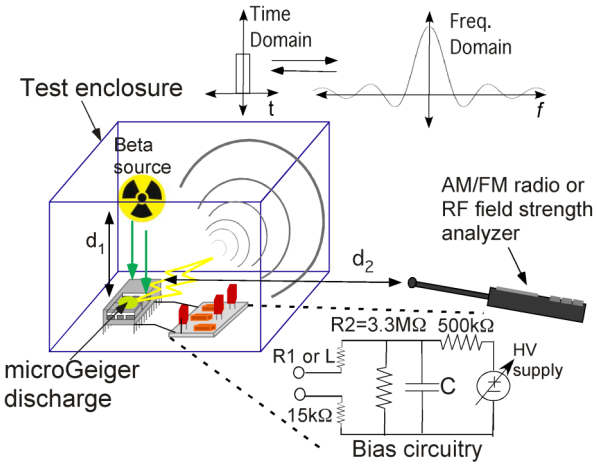

Fig. 5: *Test setup for Design A.* RF field strength analyzer (FSA) measures the wireless emissions from the micro-detector and bias circuitry. Detector to antenna distance, d_2, is fixed at 25.4 cm. Applied voltage is between 850 V and 900 V.

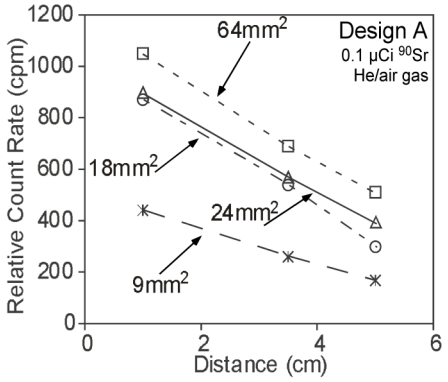

Fig. 6: Relative count rates from Design A as a function of source to detector distance, d_1, and cavity size. Four cavity sizes were tested at three separation distances [7].

During sensor operation, the RF transmission is measured using various remote transceivers, such as an RF field strength analyzer (FSA) with an 800 MHz whip antenna. The measured RF spectrum (Fig. 7) extends beyond 3 GHz with the majority of signal content existing between 5-20 rel. dBμV [8]. Compensation for the antenna gain factor (AGF) has not been taken into account. Figure 7 shows that AGF increases linearly from 23 dB to 39 dB between 100 MHz and 1.5 GHz, and remains at approximately 40 dB between 1.5 GHz to 2.0 GHz. By decreasing the bias capacitor, C, the relative signal strength as well as signal content can be significantly increased. This presents a design compromise, since a large C can accommodate a wider dynamic range of incoming beta-particles without changing the bias across the electrodes.

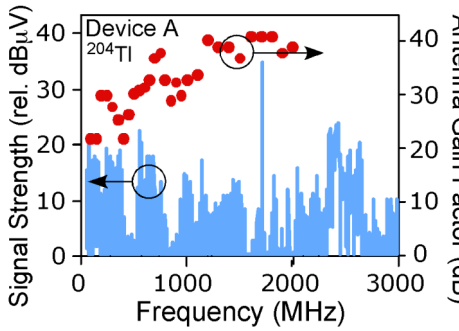

Fig. 7: RF spectra from Device A received with field strength analyzer shown with the associated antenna gain factor.

3. MICRO-DETECTOR - DESIGN B

Device Concept

A device that is even simpler to manufacture than Design A uses a planar, metal-on-glass structure (Design B). There are two electrode configurations of interest: 2- and 3-electrode geometries that use closely spaced metal electrodes electroplated on an insulating glass substrate (Fig. 8). The 3-electrode arrangement employs a high-impedance middle-electrode that separates the detection area (≈1 mm^2) into two regions: *sensing gap* and *charging gap*. The *sensing gap* located between the cathode and floating electrode has a relatively large interaction area (200X500 μm^2) and a high electric field (1-2 MV/m). Initially, weak leakage current (generally, field-emission) charges the capacitor, C_P, (Fig. 9) to a high voltage through the *charging gap,* located between the floating electrode and anode. When ionizing radiation initiates a micro-discharge within the *sensing gap*, the charge on C_P (≈1.1 pF) is dumped through the low impedance path, lowering the applied voltage and quickly quenching the discharge.

In contrast, the 2-electrode device involves the *sensing gap* alone. It can be implemented using the same microchip as the 3-electrode device. The floating electrode is hardwired to serve as the anode connection, while the cathode is still grounded.

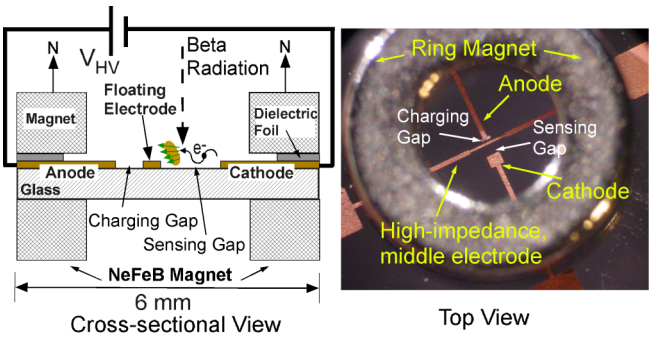

Fig. 8: (Left) Cross-section of the **3-electrode (Design B)** device sandwiched in a magnetic arrangement (explained in Sec. 4). (Right) Photograph of Design B (3-electrode, 25 μm-thick Cu) shown through magnet opening.

The 3-electrode approach results in rapid current switching, which is favorable for RF generation, because it increases the time derivative of current pulses. It also enables greater control of discharge energy, resulting in a faster response time, wider dynamic range, lower power consumption, and superior electrode durability when compared to the 2-electrode configuration. (The 2-electrode geometry is used as a control to compare performance with the 3-electrode device under similar experimental conditions.)

Preliminary gamma radiation detection using micromachined bulk metal layers has also been demonstrated [9]. Gamma rays interact with the metal, which converts them into photoelectrons. These photoelectrons consequently ionize the surrounding gas in a similar fashion as beta-particles.

Experimental Results

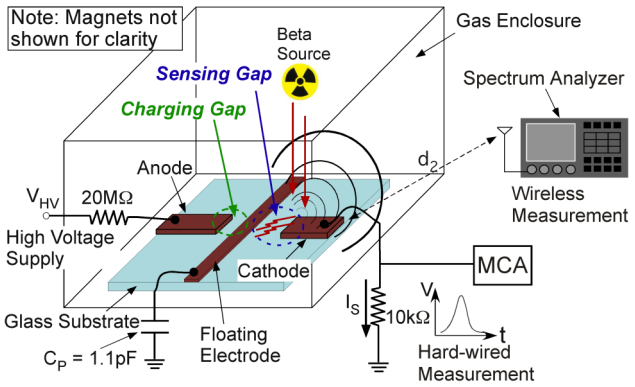

Fig. 9: *Test setup for Design B.* Hard-wired measurements require direct connection to the cathode, while wireless measurements of RF spectra use an antenna and receiver at a set distance from the detector. Source to detector distance is fixed at 8 mm, while detector to antenna distance, d_2, is varied.

For hard-wired measurements in our test set-up, current pulses (I_S) were measured by a high-speed pico-ammeter (Keithley 486) for over 100 s during device operation (Fig. 9). The 3-electrode arrangement demonstrated a 10X reduction in pulse amplitudes, as well as a faster response time compared to the 2-electrode device (Fig. 10). Figure 11 shows signal-to-noise ratios (SNR) for the 2- and 3-electrode arrangements using pulse height spectra measured with a multi-channel analyzer (MCA). SNR is defined as the ratio of count rates with and without a radiation source present. Count rates without a source present involve spontaneous electrostatic discharges (ESD) and background radiation. ESDs tend to occur more frequently when the applied voltage exceeds or nears the gas breakdown voltage. The 3-electrode arrangement shows a 10X-100X SNR improvement over the 2-electrode design for the measured range of anode bias (400-525 V). A higher SNR for the 3-electrode device allows for more reliable operation at a wider range of bias voltages.

Wireless transmissions are measured with a high frequency spectrum analyzer and an 800 MHz commercial whip antenna. Figure 12 shows total radiated power decaying with increasing detector to antenna distance, d_2.

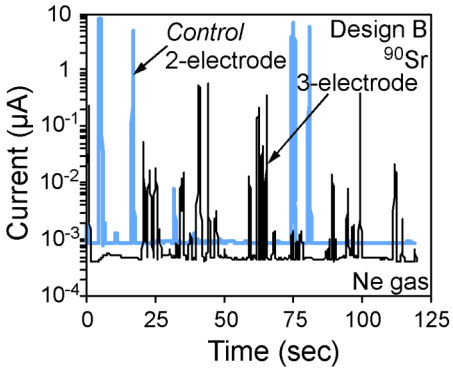

Fig. 10: Hard-wired measurement with Design B (3-electrode, Cu) showing current pulses measured by a fast pico-ammeter. Detetector-antenna spacing, d_2, was fixed at 5 cm. Control was the 2-electrode device [10].

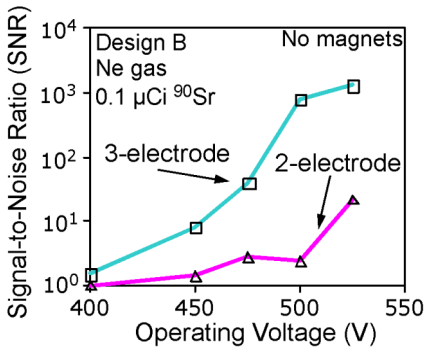

Fig. 11: Hard-wired measurement with Design B comparing SNR for 2- and 3-electrode configurations. Cu electrodes, without magnets were used and detector-antenna spacing, d_2, was fixed at 5 cm [10].

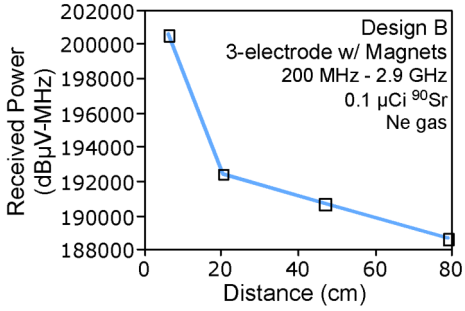

Fig. 12: Wireless measurement with Design B. Measured signal attenuation of total received wireless power spanning from 200 MHz to 2.9 GHz as a function of detector-antenna spacing. 0.1 μCi of ^{90}Sr was used.

4. Permanent Magnets

Integrating permanent magnets (NdFeB) with the micro-detector structures can enhance the RF generation. The idea is similar to a magnetron, where magnets suppress wall collisions and increase the efficiency of the electro-discharges. The ring-shaped magnets (shown in Fig. 3 and Fig. 8) are located above and below the device. The upper magnet is electrically isolated from the electrodes by an

insulating spacer. The lower magnet, placed below the glass substrate, is used to stabilize the arrangement. The magnetic field lines are positioned perpendicular to the discharge path. A particle that is moving in the presence of both an electric field and an orthogonal magnetic field, B_0, which is also consequently perpendicular to the discharge path, will experience a drift velocity, v_F, perpendicular to both fields:

$$v_F = \frac{(\mathbf{F}_\perp / q) \times \mathbf{B}}{B_0^2} \qquad (1)$$

$F_\perp$ represents the transverse force due to the electric field acting on the particle. **B** is the component of the magnetic field that is orthogonal to the electric field and q represents the charge. The particle will experience a gyrating motion, much like a spiral coil course [11]. Theoretically, the new trajectory provides an opportunity for more ion-to-neutral gas atom collisions, and thereby creates more ionized particles that can participate in the wireless transmission. Since each accelerating particle emits electromagnetic radiation, increasing the number of excited atoms can generate a stronger overall signal.

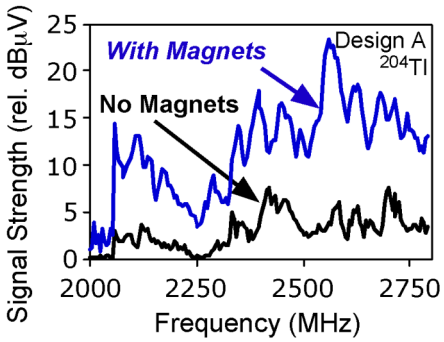

Fig. 13: (Design A) - Magnetically-enhanced RF spectrum from the Si/glass device while sensing ^{204}Tl. Control (black line) was taken without magnets [12].

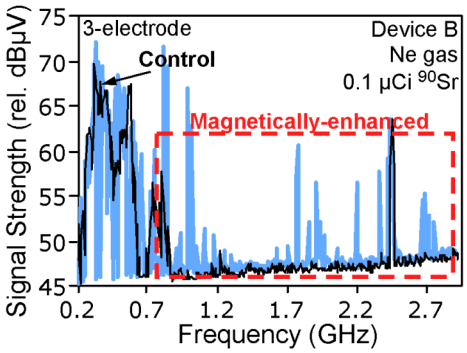

Fig. 14: (Design B) - Magnetically-enhanced RF spectrum from the 3-electrode, Cu device, while sensing ^{90}Sr. Control (black line) was taken without magnets [9].

Experimental Results

The impact of integrating permanent magnets with the Si/glass (Design A) structure can be seen in Fig. 13. A consistent increase in the RF signal spans the entire measurement bandwidth (from 2.0-2.9 GHz). Similarly, Fig. 14 shows the magnetic enhancement of the discharge spectra, while using the planar, 3-electrode (Design B) Cu device. A significant increase in higher frequency spectral strength and content are achieved in the presence of the applied magnetic field. The black lines in Fig. 13 and Fig. 14 correspond to the spectra produced in the absence of magnets (Control). Integration of rare-earth magnets can potentially be used to amplify the RF signal and increase the transmission distance without additional power demands.

5. Gas Composition & Electrode Material

The pressure and composition of the fill-gas can have a major impact on the device performance, especially in terms of the operating voltage and wireless transmissions. Gas type and pressure impact the ease of ionization and the nature of the discharge current pulse. In addition, the use of metal electrodes with higher secondary electron emission coefficients (SEEC) can increase RF performance. SEEC is defined as the number of ejected electrons per incident positive ion. These are the electrons that trigger the avalanche process in the fill-gas. By tailoring operating pressure, ratio of various fill-gases (i.e. Ne and N_2), and electrode material, RF performance and power demands can be optimized.

Experimental Results

Tests were conducted in a gas flow chamber where pressure and individual gas flow rates for Ne and N_2 were controlled. While a constant fill-gas ratio was maintained for Ne and N_2 (10:1), operating voltage was observed to scale with gas pressure (Table 1). Packaging the device in a partial vacuum can result in power savings. In Table 2, the ratio of Ne-to-N_2 was varied from 1:5 to 3:5. By increasing the Ne content (from 17% to 38%), the minimum operating voltage decreased by 200 V, without significant loss in RF performance.

Table 1: Dependence of operating voltage on chamber pressure. The 2-electrode, Cu devices with 235 μm gap spacings were tested.

Operating Voltage (V)	Pressure (Torr)
322	460
522	540
723	625

Table 2: Impact of fill-gas mixture on operating voltage and total received wireless power. Total received background noise ≈214,350 dBμV-MHz. The 2-electrode, Cu devices with 235 μm gap spacings were tested.
*Optimum operating conditions

Pressure = 737 Torr Gap spacing = 235 μm	Ratio of (Ne:N_2)		
	3:5*	2:5	1:5
Minimum operating voltage (V)	1200	1300	1400
Total received wireless power *above* background noise (dBμV-MHz)	4155	4690	4412

The total received wireless power is determined by summing the amplitudes of all frequency components

spanning the measurement bandwidth (0–4 GHz in 10 MHz intervals). RF measurements of the total received background noise spectra (without current discharges present) determine the minimum detectable wireless signal.

Micro-detectors with nickel and copper electrodes (with identical metal patterns) show comparable minimum operating voltages at 760 Torr (Table 3). However, nickel electrodes provide an increase of approximately 30% in total received wireless power compared to copper electrodes. This is likely due to the higher SEEC of Ni (≈0.015) over Cu (≈0.01) [13].

Table 3: Impact of electrode material on operating voltage and total received wireless power. Gap spacing = 235 μm. Total received background noise ≈127,786 dBμV-MHz.

Electrode Material	Cu	Ni
Min. Operating Voltage (V)	700	750
Total received wireless power *above* background noise (dBμV-MHz)	6664	8582

6. CONCLUSIONS

In this effort, we investigated RF transmissions that are produced by gas discharge-based radiation detectors during operation. Two micro-detector designs were proposed: (1) a Si/glass stack with 6 independent cavities and (2) a planar, 3-electrode copper device with a 250X500 μm^2 active footprint electroplated onto a glass substrate. The presence of a third, high-impedance middle electrode can improve detector performance by decreasing the resulting current pulses and increasing the switching or recovery speed. Smaller current pulses result in less sputtering of the electrodes, which increases device performance and reliability. The faster switching time increases the spectral strength of the consequent RF transmission because it is directly related to the derivative of the current pulse. Each detector structure has integrated miniaturized magnets to increase the inherent emission characteristics without additional power demands.

Preliminary tests investigated the effect of electrode material, fill-gas type, and pressure on the operating voltage and RF performance. Nickel electrodes outperformed copper electrodes by nearly 30%, which is attributed to its higher SEEC. Targeting higher atomic materials for the electrode structure can result in greater amplification in pulse heights as well as stronger RF emissions. In addition, since operating voltage scales with gas pressure, packaging the micro-detector under partial vacuum can lower power demands. Commercial packaging solutions have been considered and preliminary data indicate negligible impact on the RF performance. Gas mixtures of neon and nitrogen show that higher neon content results in lower operating voltages, while maintaining similar RF performance. In the future, these RF transmissions can be applied as a communication method for the wireless detection of radiological chemicals.

ACKNOWLEDGEMENTS

The authors gratefully acknowledge Prof. Ranjit Gharpurey's contributions to early versions of these devices and Dr. Bhaskar Mitra for his contribution to the 3-electrode configuration. This work was supported primarily by the Engineering Research Centers Program of the National Science Foundation under Award Number EEC-9986866. The facilities used for this research include the Michigan Nanofabrication Facility (MNF) at the University of Michigan. Y.G. acknowledges support through the IR/D program while working at the National Science Foundation. The findings do not necessarily reflect the views of the NSF.

REFERENCES

[1] R.J. Nemzek, "Distributed sensor networks for detection of mobile radioactive sources," *IEEE Transactions on Nuclear Science*, 51(4), pp. 1693-1700, Aug. 2004.

[2] R. Kyker et al, "Hybrid Emergency Radiation Detection, a wireless sensor network application for consequence management of a radiological release," *Digital Wireless Communications VI,* 2004.

[3] G.F. Knoll, "Radiation Detection and Measurement," *John Wiley and Sons,* 2000, pp. 161.

[4] T. Francke and P. Vladimir, "Micropattern gaseous detectors," Pres. at *42nd INFN ELOISATRON Project Workshop*, Erice, Italy, Sept. 2003.

[5] J.E. Brittain, "Electrical engineering Hall of Fame: Guglielmo Marconi," *Proceedings of the IEEE*, 92(9), Aug 2004, pp. 1501-1504.

[6] A.G. Heaton and J.H. Reeves, "Microwave radiation from discharges," *3rd Intl. Conf. on Gas Discharges*, Sept. 1974, pp. 73-77.

[7] C.G. Wilson, et al., "A microfabricated beta-particle detector with dual cavities for energy spectroscopy," *IEEE Intl. Conf. on MEMS*, Miami, Jan. 2005.

[8] C.K. Eun, et al., "Controlling ultra wideband transmissions from a wireless micromachined Geiger counter," *IEEE Intl. MEMS Conf.*, Jan. 2006, p. 570-3.

[9] C.K. Eun and Y.B. Gianchandani, "A micromachined wireless gamma radiation detector using bulk metal conversion layers," *Solid-State Sensors, Actuators & Microsys. Workshop*, Hilton Head, Jun. 2006, *in press.*

[10] C.K. Eun, et al., "A magnetically enhanced 3-electrode wireless micro-Geiger counter," *IEEE Intl. MEMS Conf.,* Jan. 2007, pp. 599-602.

[11] M. A. Lieberman and A. J. Lichtenberg, *Principles of Plasma Discharges and Materials Processing*, John Wiley and Sons, Inc. 2nd Edition, 2005.

[12] C.K. Eun, et al., "A magnetically enhanced wireless micro-Geiger counter," *Solid-State Sensors, Actuators & Microsys. Workshop*, Hilton Head, Jun. 2006, pp. 236-9.

[13] P. Guillot, et al., "Secondary electron emission coefficients of standard samples for GDOES," *Surface and Interface Analysis,* vol. 35, pp. 590-592, 2003.